DOI 10.1007/s10812-022-01365-x
Journal of Applied Spectroscopy, Vol. 89, No. 2, May, 2022 (Russian Original Vol. 89, No. 2, March–April, 2022)

COMBINED MULTISPECTROSCOPIC AND MOLECULAR DOCKING ASSESSMENTS TO THE EFFECT OF AN ANTICONVULSANT, OXCARBAZEPINE ON HUMAN SERUM ALBUMIN CONFORMATION AND ITS BINDING PROPERTIES

M. Manjushree[a,b] and H. D. Revanasiddappa[b,*]

UDC 543.42:547.962.3

Elimination and distribution of drugs are affected by human serum albumin (HSA) interaction. In children and adults, specific types of seizures are controlled by oxcarbazepine (OXZ) alone or in combination with other medications. However, the OXZ interaction with HSA was probed through 3D fluorescence, emission fluorescence, UV-Vis spectroscopy, and molecular docking. OXZ statically quenched the HSA fluorescence spontaneously and exothermically. Thermodynamic parameters revealed the involvement of hydrogen bonds together with van der Waals forces. Molecular docking inspections confirmed that OXZ is bound to site I of HSA. Strong binding with OXZ (of K_b order 10^5 L/mol) reduced the secondary, micro-environmental, and conformational structures of HSA, suggesting that it unfolds. Thus, the assessment of such conformational details of OXZ–HSA binding is pivotal in surveying the efficacy of OXZ as a therapeutic operator and interpreting its pharmacokinetic properties.

Keywords: *binding interaction, secondary structure, energy transfer, molecular docking, oxcarbazepine.*

Introduction. Oxcarbazepine (OXZ) is a medication employed to treat bipolar disorder and epilepsy. For epilepsy OXZ is utilized for both focal and generalized seizures. Patients had not succeeded with other treatments for bipolar disorder; OXZ also served both alone and in extension therapy. Frequent side effects are vomiting, nausea, dizziness, double vision, drowsiness, and difficulty walking. Severe side effects are liver problems, anaphylaxis, abnormal heartbeat, suicide, and pancreatitis. The baby may be harmed during pregnancy if the mother is on OXZ treatment [1–4].

Human serum albumin (HSA) is a vital plasma protein in humans, which has numerous functions throughout the circulation, including transportation of various ligands and regulation of colloid osmotic pressure. HSA furthermore binds to numerous drug molecules, which are an imperative factor for determination of drug pharmacokinetics, including elimination and distribution [5, 6].

Hence, the binding interaction between OXZ and HSA was studied by diverse spectroscopic and molecular docking approaches.

Methods. Commercial HSA (agarose gel electrophoresis, ≥97%) and OXZ (high-performance liquid chromatography, ≥98%) were obtained from Sigma-Aldrich (St. Louis, MI, USA). Analytical standards were exercised to other chemicals. The whole examinations were practiced with Tris buffer at a pH of 7.40 produced from double-distilled water. HSA at $1.0\cdot10^{-4}$ mol/L while site markers, OXZ at $1.0\cdot10^{-3}$ mol/L as the stocks. Human serum albumin ($1.25\cdot10^{-6}$ mol/L) UV-Vis absorption spectra in the presence of OXZ with different concentrations (0.0, 0.25 up to $2.50\cdot10^{-6}$ mol/L) were performed on a UV-visible spectrophotometer DU 730 (Beckman Coulter, Brea, CA, USA) conducted within a wavelength range of 205–330 nm at 305 K. The CD analysis was made with a J-815 CD spectropolarimeter (Jasco, Tokyo, Japan) for HSA ($1.25\cdot10^{-6}$ mol/L) in OXZ ($37.5\cdot10^{-6}$ mol/L) absence and presence at 305 K. A 200- to 240-nm scanning wavelength, 10-mm cell length, and 100-nm/min scanning speed were applied while recording the spectrum. Three-dimensional (3D) fluorescence spectra were measured in emission/excitation (250–500/200–380 nm) wavelength for the OXZ–HSA system and HSA ($1.25\cdot10^{-6}$ mol/L) at 305 K. The OXZ concentration was $11.25\cdot10^{-6}$ mol/L.

*To whom correspondence should be addressed.

[a]Department of Chemistry, MMK & SDM Mahila Mahavidyalaya, Krishnamurthypuram, Mysuru, Karnataka, India; [b]Department of Chemistry, University of Mysore, Manasagangothri, Mysuru, Karnataka, India; email: hdrevanasiddappa@yahoo.com. Abstract of article is published in Zhurnal Prikladnoi Spektroskopii, Vol. 89, No. 2, p. 286, March–April, 2022.

Complete fluorescence analysis was carried out using a fluorescence spectrophotometer F-4600 (Hitachi, Tokyo, Japan) equipped with a Xenon lamp of 150 W. HSA ($1.25 \cdot 10^{-5}$ mol/L) with different OXZ concentrations (0.00, 0.25 up to $2.50 \cdot 10^{-6}$ mol/L) was employed for emission fluorescence measurements at 297, 305, and 313 K in emission wavelengths from 290 to 500 nm and excitation at 295 nm. Slit wavelengths for excitation and emission were 10 nm. A water bath was maintained to obtain the required temperatures. The fluorescence intensity of each one was corrected by the inner filter effect for absorption of excited light and re-absorption of emitted light.

Energy optimization and minimization were applied to the structures of OXZ (PMID: 34312) and HSA (PDB ID: 1AO6) by Marvin View and GROMOS96 force field respectively. Seventy runs across 60-grid size were applied to three binding sites in all directions for the docking analysis on Autodock Tools. All docking evaluations were done using the Lamarckian genetic algorithm and the binding visualizations were made by Discovery Studio.

Results and Discussion. *UV-Vis spectroscopic characteristics.* The HSA UV-Vis absorption spectrum represented in Fig. 1a demonstrating two absorption bands was strong at 212 nm assigned to the HSA backbone and weak at 279 nm owing to aromatic amino acids respectively [7]. By varying the OXZ concentration, a noticeable increase in the absorbance peak intensity at each peak position, including a blue shift of about 2 nm (for 212 nm) and 12 nm (for 279 nm) in maximum wavelength was pointed out, which indicates that there was a modification in the HSA conformational framework due to the formation of the OXZ–HSA complex. Furthermore, micro-environmental alterations occurred to aromatic amino acids [8].

CD measurements. Figure 1b represents the HSA CD spectrum with and without OXZ, explaining $\pi \rightarrow \pi^*$ (at 208 nm) and $n \rightarrow \pi^*$ (at 222 nm) transitions, which are characteristic of HSA α-helical for peptide bond [9]. Both peaks for HSA decreased noticeably without imposing any shift after the addition of OXZ. This establishes the HSA secondary structural modifications induced by the OXZ binding interaction: α-helix (from 57.01 to 52.90%), β-sheet (2.26 to 0.08%), random coils (9.53 to 4.40%), and β-antiparallel (2.94 to 2.12%) of HSA decreased, whereas β-turn (28.17 to 40.66%) increased upon interaction with OXZ; these were evaluated using BeStSel software. When compared with the reported literature, such slight modifications in the secondary structural content of HSA, upon binding with small ligands, are inconsistent with the present investigation [10–12].

3D fluorescence analysis. HSA conformational changes by interaction with OXZ were investigated from 3D fluorescence (Fig. 2) spectra. The peaks [13] are reduced from HSA to the OXZ–HSA system at "a" for $\lambda_{ex} = \lambda_{em}$ (Rayleigh scattering) (1044 → 1093 to 920.9 → 1039), "b" for $2\lambda_{ex} = \lambda_{em}$ (second-order scatte-ring) (325.7 to 257.7), "1" for transition of $n \rightarrow \pi^*$ (Tyr/Trp) (706.3 to 637.2), and "2" indicating $\pi \rightarrow \pi^*$ transition (peptide chain) (369.8 to 321.6). This demonstrated that the OXZ binding with HSA affects the polypeptide backbone and microenvironments of Trp/Tyr of HSA.

Fluorescence quenching mechanism. Various molecular interactions — molecular rearrangements, collision quenching, energy transfer, ground-state formed complex, excited-state reactions — induce decreasing fluorescence intensity of proteins. Quenching refers to fluorescence quenching. Dynamic (excited-state reactions) and static (ground-state complex) are the usual quenching mechanisms that differ by lifetime measurements and temperature dependence. Quenching constants are increased by a rise in temperature for dynamic whereas the opposite is true for static. Figure 3a shows a strong emission peak at 340 nm ($\lambda_{ex} = 295$ nm) with a regular decreased intensity, which is representative of Trp. Thus, the binding of OXZ quenched the intrinsic fluorescence of Trp-214 in HSA.

If dynamic quenching occurs to the OXZ–HSA system, the Stern–Volmer equation is analyzed for fluorescence data [14]:

$$F_0/F = 1 + k_q\tau_0[Q] = 1 + K_{SV}[Q], \quad (1)$$

$$k_q = K_{SV}/\tau_0, \quad (2)$$

where k_q and τ_0 are the bimolecular quenching rate constant ($2.0 \cdot 10^{10}$ L·mol^{-1}·s^{-1}) and fluorophore average lifetime without OXZ (~$2.7 \cdot 10^{-9}$ s), respectively; F_0 is the fluorescence intensity without OXZ, F is the fluorescence intensity with OXZ, [Q] is the OXZ concentration, and K_{SV} is the Stern–Volmer quenching constant. The Stern–Volmer plot from Fig. 3b gives K_{SV} values their k_q values were calculated which decreased clearly at higher temperatures (297, 305, and 313 K) listed in Table 1. Also, k_q values of order 10^{13}.

All these results illustrate that the quenching process by OXZ for HSA was probably statically controlled, resulting from formation of the OXZ–HSA complex.

Furthermore, quenching data were examined using the modified Stern–Volmer equation to evaluate an effective static quenching constant (K_a) for the accessible fluorophores [15]:

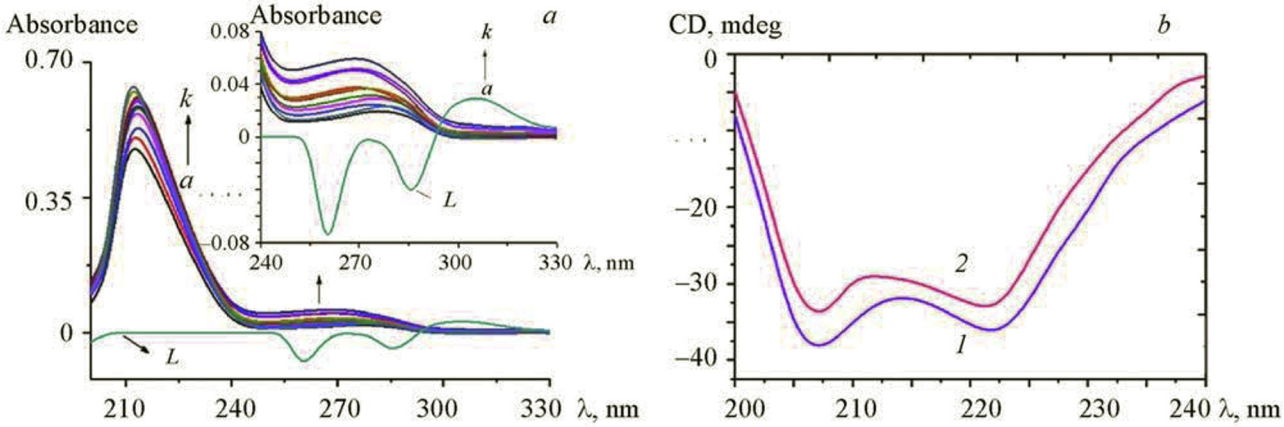

Fig. 1. (a) Alteration of HSA ($1.25 \cdot 10^{-6}$ mol/L) UV-Vis spectrum with increased OXZ concentrations (0.0, 0.25 up to $2.50 \cdot 10^{-6}$ mol/L) at 305 K, (b) free HAS and OXZ–HAS system CD spectrum, obtained in a concentration of HAS of $1.25 \cdot 10^{-6}$ mol/L (*1*) and for OXZ it was $37.5 \cdot 10^{-6}$ mol/L (*2*).

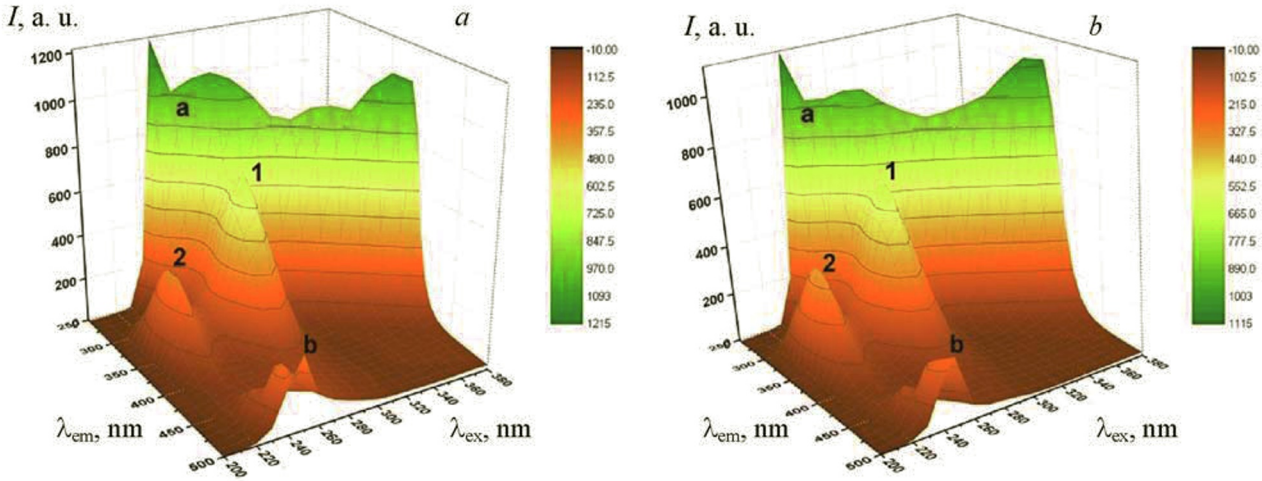

Fig. 2. 3D fluorescence spectra at 305 K: (a) HSA alone ($1.25 \cdot 10^{-6}$ mol/L) and (b) OXZ–HSA system where OXZ concentration was $11.25 \cdot 10^{-6}$ mol/L.

$$F_0/(F_0 - F) = (1/f_a) + (1/K_a f_a[Q]) \,, \tag{3}$$

where f_a is the accessible fluorescence fraction. The obtained K_a values from the modified Stern–Volmer plot (Fig. 3c and Table 1) decrease as temperature increases, which is in accordance with the K_{SV} values mentioned above.

Binding parameters. Drugs persist in peripheral dissemination as bound and free (unbound) to protein following the principle of reversible equilibrium and law of mass action. Frequently, for a given drug, equilibrium exists between the free drug and the protein-bound drug. The following equation defines this equilibrium [16]:

$$\log [(F_0 - F)/F] = \log K_b + n \log [Q]. \tag{4}$$

The values of K_b (binding constant) and n (number of binding sites) are examined from the intercept and slope of $\log [(F_0 - F)/F]$ versus $\log [Q]$ plot depicted in Fig. 3d. In plasma, the amount of drug distribution is generally determined

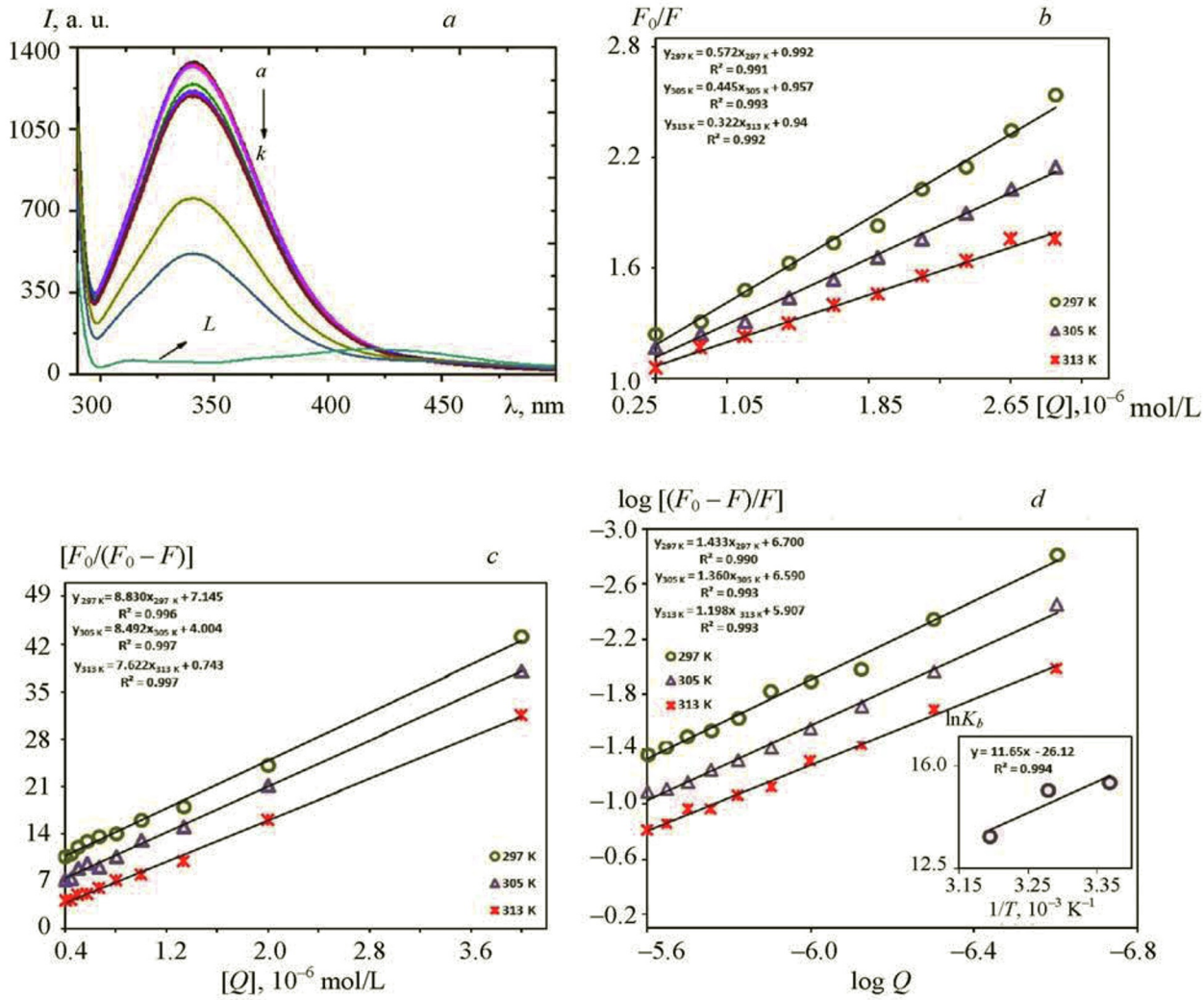

Fig. 3. OXZ–HSA system at various temperatures: fluorescence emission (a), Stern–Volmer (b), modified Stern–Volmer (c), and binding parameters (d), inset shows Van't Hoff plots.

TABLE 1. Various Quenching Constants to OXZ–HSA System at Distinct Temperatures

Temperature, K	K_{SV},10^5 L/mol	k_q,10^{13} L·mol^{-1}·s^{-1}	K_a,10^5 L/mol
297	5.72 ± 0.10	21.18 ± 0.04	8.09 ± 0.05
305	4.45 ± 0.02	16.48 ± 0.06	4.72 ± 0.01
313	3.22 ± 0.07	11.92 ±0.08	0.97 ± 0.04

by K_b, where strong binding diminishes free drug concentrations, making it inaccessible to the action mechanism whereas weak binding could lead to poor distribution/short lifetime. The reduction of the stability of the OXZ–HSA complex occurred because of decreased K_b values with elevated temperatures, as noted in Table 2. Moreover, values of n are nearly unity, which might signify that only one OXZ molecule binds to HSA.

Binding modes. In view of K_b dependence on temperature, thermodynamic parameters were analyzed to characterize the dominating binding forces (van der Waals, electrostatic, hydrogen bond, and hydrophobic) on OXZ–HSA interaction

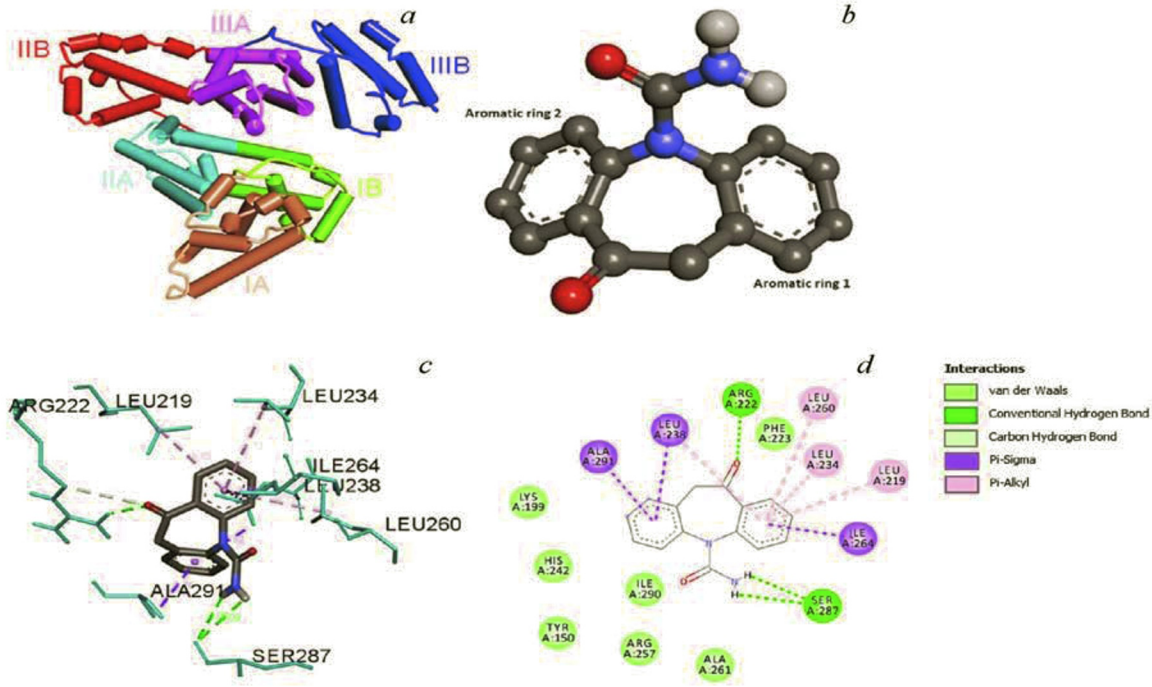

Fig. 4. (a) HSA, (b) OXZ, (c) OXZ interacted at site I of HSA and (d) 2D structure of (c).

TABLE 2. OXZ–HSA system at Various Temperatures Comprising Binding and Thermodynamic Parameters

Temperature, K	K_b, 10^5 L/mol	n	ΔG, kJ/mol	ΔH, kJ/mol	ΔS, kJ/mol
297	50.12 ± 0.08	1.433	–32.36	–96.86	–217.16
305	38.90 ± 0.07	1.360	–30.62	–	–
313	8.07 ± 0.06	1.198	–28.88	–	–

[17]. Thermodynamic parameters evident for authenticating binding modes are (ΔS) entropy change and (ΔH) enthalpy change predicted by the Van't Hoff plot (inset of Fig. 3d) using the following equation and are ordered in Table 2:

$$\text{l ln } K_\text{b} = (-\Delta H/RT) + (\Delta S/R),\ \Delta G = \Delta H - T\Delta S\ . \quad (5)$$

Negative ΔH and ΔS (Table 2) associated with van der Waals and hydrogen bonds respectively as a force to the OXZ–HSA interaction. This interaction process proceeded spontaneously (negative ΔG), exothermically (negative ΔH), and entropy-driven ($\Delta H < \Delta S$).

Molecular docking to the OXZ–HSA system. Based on cluster analysis, the best docking results for three binding sites in HSA for OXZ are shown in Fig. 4. As could be seen, OXZ is satisfactorily situated inside site I (sub-domain IIA) formed by helices, which is predicted from the obtained least binding energy and largest cluster mode in correlation with the other two sites. OXZ binds to HSA through various amino acids by interacting forces, which are van der Waals: PHE223, LYS199, HIS242, ILE290, TYR150, ARG257, and ALA261; conventional hydrogen bond: SER287:O — H11, SER287:O — H12, and ARG222:HH12 — O1; carbon hydrogen bond: ARG222:CD — O1; pi — sigma: ALA291:CD — aromatic ring 1; LEU238:CD1 — aromatic ring 1, and ILE264:CD1 — aromatic ring 2; Pi-Alkyl: LEU238:(CD1-CG-CD2)-aromatic ring 2; LEU260: (CD1-CG-CD2)-aromatic ring 2; LEU234: (CD1-CG-CD2)-aromatic ring 2; and LEU219: (CD1-CG-CD2)-aromatic ring 2. Moreover, OXZ surrounds more polar and ionic amino acids in contrast to hydrophobic amino acids. Hence, the major accompanying forces are van der Waals and hydrogen bonds. Concurrently, these results are in agreement with the executed fluorescence quenching valuations [18–20].

Conclusions. Under physiological conditions, the interaction between OXZ and HSA was examined using UV-Vis, CD, 3D fluorescence, emission fluorescence spectroscopy, and molecular docking techniques. The formed OXZ–HSA complex was ascertained at IIA sub-domain of HSA with dominant hydrogen bonds combined with van der Waals forces by a static quenching mechanism. A modified conformational and secondary structure of HSA was achieved after OXZ interaction. Clearly, these results cannot be merely generalized. Consequences of molecular docking could effectively be applied in a thorough investigation of binding sites for HSA, and all determined parameters were in agreement with experimental entities.

Acknowledgments. M. Manjushree specially thanks UGC–BSR, India for awarding fellowship, and the Management of MMK & SDM Mahila Mahavidyalaya, Krishnamurthypuram, Mysuru for their fruitful support. The authors thank CATERS, CSIR-CLRI, Chennai and IOE, Mysuru for CD measurements and other instrumental facilities respectively.

REFERENCES

1. A. B. Kobetz, A. S. Carrazana, and J. Enrique, *Clin. J. Pain*, **20**, 174–178 (2004).
2. G. Serdaroglu, S. Kurul, S. Tutuncuoglu, E. Dirik, and B. Sarioglu, *Pediatr. Neurol.*, **28**, 37–41 (2003).
3. E. Şavka, O. Bolukbasib, A. Akyol, and G. Karamana, *J. Am. Acad. Dermatol.*, **45**, 630–632 (2001).
4. M. C. Rouan, J. B. Lecaillon, J. Godbillon, E. Menard, T. Darragon, E. Meyer, O. Kourilsky, D. Hillion, J. C. Aldigier, and P. Jungers, *Eur. J. Clin. Pharmacol.*, **47**, 161–167 (1994).
5. T. J. Peters, *All About Albumin*, Academic Press, London (1996).
6. O. J. M. Bos, M. J. E. Fischer, J. Wilting, and L. H. M. Janssen, *Biochem. Pharmacol.*, **38**, 1979–1984 (1989).
7. D. Zhang, X. Zhang, Y. C. Liu, S. C. Huang, Y. Ouyang, and Y. J. Hu, *J. Mol. Liq.*, **258**, 155–162 (2018).
8. N. Sudha, Y. Sameena, S. Chandrasekaran, I. Enoch, and D. Premnath, *Spectrosc. Lett.*, **48**, 112–119 (2015).
9. M. Kumari, J. K. Maurya, M. Tasleem, P. Singh, and R. Patel, *J. Photochem. Photobiol. B Biol.*, **138**, 27–35 (2014).
10. B. Ahmad, S. Parveen, and R. H. Khan, *Biomacromolecules*, **7**, 1350–1356 (2006).
11. Y. Moriyama and K. Takeda, *Langmuir*, **15**, 2003–2008 (1999).
12. T. K. Maiti, K. S. Ghosh, and J. Debnath, *Int. J. Biol. Macromol.*, **38**, 197–202 (2006).
13. S. R. Feroz, S. B. Mohamad, Z. S. D. Bakri, S. N. A. Malek, and S. Tayyab, *PLoS One*, **8**, e76067 (2013).
14. Z. Cheng, *J. Luminescence*, **132**, 2719–2729 (2012).
15. S. Lehrer, *Biochemistry*, **10**, 3254–3263 (1971).
16. C. D. Kanakis, P. A. Tarantilis, M. G. Polissiou, S. Diamantoglou, and H. A. Tajmir-Riahi, *J. Mol. Struct.*, **798**, 69–74 (2006).
17. S. N. Timasheff, in: *Proteins of Biological Fluids*, Ed. H. Peeters, Pergamon Press, Oxford (1972).
18. G. M. Morris, R. Huey, W. Lindstorm, M. F. Sanner, R. K. Belew, D. S. Goodsell, and A. J. Olson, *J. Comput. Chem.*, **30**, 2785–2791 (2009).
19. B. K. Paul, A. Samanta, and N. Guchhait, *J. Phys. Chem. B*, **114**, 6183–6196 (2010).
20. S. Y. Huang, S. Z. Grinter, and X. Zou, *Phys. Chem. Chem. Phys.*, **12**, 12899–12908 (2010).